Supporting Information for

Biophysical Characterization of Fluorotyrosine Probes Site-Specifically Incorporated into Enzymes: *E. coli* Ribonucleotide Reductase As an Example

Paul H. Oyala[§], Kanchana R. Ravichandran[†], Michael A. Funk[†], Paul A. Stucky[§], Troy A. Stich [§], Catherine L. Drennan[†,‡,&,*], R. David Britt[§,*], JoAnne Stubbe[†,‡, *]

[*]To whom correspondence should be addressed. cdrennan@mit.edu, rdbritt@ucdavis.edu, stubbe@mit.edu

[§] Department of Chemistry, University of California, Davis, One Shields Avenue, Davis, CA 95616, United States

[†] Department of Chemistry and [‡] Department of Biology, Massachusetts Institute of Technology, 77 Massachusetts Avenue, Cambridge, MA 02139, United States

[&] Howard Hughes Medical Institute, Massachusetts Institute of Technology, 77 Massachusetts Avenue, Cambridge, MA 02139, United States

SUPPORTING INFORMATION TABLE OF CONTENTS

Reconstitution of the diferric-(2,3,6)F_3Y• cofactor at 25 °C monitored by RFQ-EPR spectroscopy. Rapid freeze-quench (RFQ) experiments were conducted on an Update Instruments 1019 syringe ram unit and a model 715 Syringe Ram controller equipped with a Lauda RM6 circulating water bath set at 25 °C as previously described.[1] Apo (2,3,6)F_3Y-β2 (80 μM) containing 5 equiv. ferrous ammonium sulfate in anaerobic buffer was loaded into one syringe and mixed with an equal volume of O_2 saturated 50 mM HEPES pH 7.6, 5% glycerol contained in the second syringe. The reaction mixture was aged for varying times (23 ms–60 s), sprayed into liquid isopentane (140°C) and the crystals were packed into EPR tubes for analysis by X-band EPR spectroscopy. The spectrum of 2,3,6-F_3Y• at 0.8 s was subtracted from the composite spectrum at each of the early time points (23 ms, 83 ms and 256 ms). The net spectrum was then re-integrated to quantitate the amount of intermediate X.

TABLE S1. Components of the Modified Bridge Transmitter in Figure S2.

Number	Manufacturer	Model	Details
1	Nexyn Corp.	NXOS-XO-400.000	PLDRO, 7.647 GHz, 20 dBm out
2,8	Hewlett-Packard	8761A	SPDT latching switch
3,43,47	Mini-Circuits	BW-S	DC-18 GHz, fixed precision, 2 W
4	Mac Technology	P8206-2	7-12.4 GHz, 20 dB isolation
5	S.M. Electronics	MP8246-2	2-8GHz, 20 dB isolation
6	Narda Microwave	4015C-10	7-12.4 GHz, 10 dB coupling
7	Narda Microwave	HP-0955-0111	5.9-12.4 GHz, 16dB coupling
9	Marki Microwave	FLP-0960	LPF, 9.6 GHz is 3dB cutoff
10,33	Narda Microwave	INA-8010	8-10 GHz, 23 dB isolation
11,12	XMA Corp.	XMAPD10-2-8-4S	2-8 GHz, 18 dB isolation
13-16	Narda Microwave	4915	7-10 GHz, 20 dB isolation
17-21	Arra Microwave	6814-40	8-12.4 GHz, variable level set, 40 dB
22-25	Arra Microwave	9426A	DC-18 GHz, var. mech. phase shifter
26-30	Hittite Microwave	HMC-C019	SPST MESFET, DC-20 GHz, 3 dB IL
31	Ditom Microwave	DF6113	7.4-8.4 GHz, 15 dB isolation
32	Mini-Circuits	ZVA-183-S+	0.7-18 GHz, 26 dB gain, 24 dBm out
34	Avantek	AFT-8462	4-8 GHz, 13 dB gain, 20 dBm out
35	S.M. Electronics	MP8245-2	4-8 GHz, 20 dB isolation
36	Marki Microwave	T30838LN	8-38 GHz LO/RF, 0.01-10 GHz IF
37	Marki Microwave	FB-3270	BPF, 32.70±3.95 GHz
38	Narda Microwave	4015C-6	7-12.4 GHz, 6 dB coupling
39	Hereley-CTI	XS-7314	Synth., 7.647±0.300GHz, 10Hz res, 15 dBm out
40	Spincore	PBESR-Pro-400	Word generator, 21ch, 400 MHz
41	Marki Microwave	DA-0408K	Freq. ×2, 8-16 GHz, 20 dBm out
42	Nexyn Corp.	NXD0765019103742	Freq. ÷4, 1.911 GHz, 13 dBm out
44	Marki Microwave	M2B0218LP	3-17 GHz LO/RF, 2-10 GHz IF
45	Marki Microwave	FB-1575	BPF, 15.75±1.25 GHz
46	Marki Microwave	FB-0955	BPF, 9.55±0.65 GHz
48	Marki Microwave	M2B0226LP	2-18 GHz LO/RF, 1-10 GHz IF
49	Marki Microwave	FB-2480	BPF, 24.8±3.7 GHz
50	Marki Microwave	AP-0125EZP	1-25 GHz, 26 dB gain, 20 dBm out
51	Jani Electronics	HMC863LP4E	Hittite IC on PCB, 22-27 GHz, 27 dBm
52	Narda Microwave	4917	18-26.5 GHz, 17 dB isolation
53	ATM Microwave	AF-068-20	14-26.5 GHz, freq. flat, variable, 20 dB
54	Virginia Diodes	VDI-AMC-371	Freq. x4, 130 GHz, 23.2 dBm out
55	Aerowave	06-1890	WR6, 90° E-plane, ALMA flange
56	Cernex	CWS1101701235	WR6, waveguide 4-port manual switch
57	HF EPR Instr.	—	WG circulator, original equipment

TABLE S2. Specific activity (SA) of F_nY•-β2 as determined by spectrophotometric and radioactive assays for nucleotide reduction. wt-β2 and (3,5)F_2Y•-β2 assays are linear with time, while those with (2,3,5)F_3Y•-β2, (2,3)F_2Y•-β2 and (2,3,6)F_3Y•-β2 are non-linear with time after 5 min, 5 min, and 45 s respectively.

β2	Yield (mg protein/g cell)	Maximum Y•/β2	SA (nmol/min/mg)	% wt
wt	30	1.2	6900 ± 350	100
(3,5)F_2Y	30	1.0	5780 ± 230	84
(2,3,5)F_3Y	10-15	0.9	1300 ± 100	19
(2,3)F_2Y	5-7	0.8	450 ± 20	6.5
(2,3,6)F_3Y	7-12	1.2[a]	350 ± 10[b]	5

[a] A maximum of 1.2 F_3Y•/β2 is obtained within 300 ms of reconstitution (determined by RFQ-EPR spectroscopy, Figure S4). However, roughly half of the total radical decays within 2 min of reconstitution, while the remaining amount is stable for at least 30 min.
[b] The reported SA is that of (2,3,6)F_3Y•-β2 containing 0.4 F_3Y•/β2.

TABLE S3: Data collection by XRD and model statistics for wt-β2 and F_nY-β2 variants. Values in parentheses represent the highest resolution bin. The test set for each dataset contained 5% of the total reflections and was matched between datasets.

Data collection and processing

R2 variant	wild type	3,5-F_2Y122	2,3-F_2Y122	2,3,5-F_3Y122	2,3,6-F_3-Y122
SBgrid accession number*	226	230	228	229	227
Resolution (Å)	50-2.05 (2.09-2.05)	50-2.25 (2.29-2.25)	50-1.95 (1.98-1.95)	50-2.40 (2.44-2.40)	50-2.25 (2.29-2.25)
Wavelength (Å)	0.9795	0.9792	0.9795	0.9795	0.9795
Completeness (%)	97.3 (76.2)	99.6 (95.8)	97.3 (98.9)	98.7 (91.0)	99.7 (95.8)
<I/σI>	25.0 (2.1)	27.7 (1.3)	17.4 (1.7)	30.3 (1.4)	25.6 (1.0)
R_{merge}	0.036 (0.401)	0.076 (0.675)	0.072 (0.711)	0.050 (0.929)	0.063 (>1)
Unique reflections	31952 (1228)	25037 (1185)	37183 (1866)	20961 (951)	25083 (1198)
Redundancy	3.5 (2.7)	10.1 (7.0)	5.1 (5.1)	9.7 (6.8)	9.1 (7.9)
$CC_{1/2}$	0.92	0.84	0.73	0.74	0.68

Model refinement

Protein DataBank (PDB) ID	5CI4	5CI0	5CI1	5CI3	5CI2
Resolution (Å)	50-2.05 (2.09-2.05)	50-2.25 (2.34-2.25)	50-1.95 (2.00-1.95)	50-2.40 (2.52-2.40)	50-2.25 (2.34-2.25)
R_{work}, R_{free}	0.188, 0.221	0.181, 0.212	0.154, 0.183	0.166, 0.215	0.172, 0.197
Protein atoms	2911	2850	2924	2929	3095
Fe atoms	2	2	2	2	2
Water molecules	211	201	209	209	209
RMSD bond length (Å)	0.008	0.003	0.014	0.007	0.005
RMSD bond angle (º)	0.991	0.688	1.327	0.825	0.738
Rotamer outliers (%)	1.55	0.32	0.93	1.25	0.95
Ramachandran plot (%)					
Most favored	98.59	98.55	98.87	98.59	98.86
Additionally allowed	1.41	1.45	1.13	1.41	1.14
Disfavored	0.00	0.00	0.00	0.00	0.00
Average B factors (Å^2)					
All protein atoms	83.2	72.6	49.4	99.2	80.4
$[Fe_2O]^{2+}$ cluster	62.7	49.4	27.6	64.8	60.2
F_nY_{122} or Y_{122}	64.5	55.0	31.8	82.9	64.3
Water	84.4	73.5	48.6	102.5	85.3

TABLE S4. Cartesian Coordinates (Å) for Geometry Optimized Model of Phenoxyl Radical

Atom	x	y	z
C	2.779662	1.236026	-0.014719
C	1.403545	1.253344	0.001115
C	0.638305	0.018866	0.011029
C	1.400968	-1.217365	0.001351
C	2.776996	-1.202754	-0.014465
C	3.500061	0.015918	-0.019757
C	5.005008	0.013910	0.000862
H	0.837376	-2.145942	0.003523
O	-0.618686	0.020129	0.024065
H	0.842334	2.182692	0.003154
H	3.334770	2.171506	-0.024805
H	3.330132	-2.139499	-0.024346
H	5.381220	0.001009	1.034117
H	5.416136	0.907375	-0.480488
H	5.413987	-0.869181	-0.501247

TABLE S5. Cartesian Coordinates (Å) for Geometry Optimized Model of (2,3)F_2Y•

Atom	x	y	z
C	2.782922	1.175849	0.064240
C	1.406153	1.201415	0.066663
C	0.624744	-0.027792	-0.001096
C	1.394924	-1.256264	-0.070211
C	2.770480	-1.241814	-0.070431
C	3.504091	-0.030878	-0.003404
C	5.005599	0.006740	-0.001670
H	0.829774	-2.180941	-0.121477
O	-0.626024	-0.000282	0.001547
F	0.759859	2.361329	0.131439
F	3.466158	2.335137	0.128071
H	3.325516	-2.174401	-0.122924
H	5.387469	0.483616	0.909487
H	5.386817	0.595534	-0.844984
H	5.423334	-1.001213	-0.065859

TABLE S6. Cartesian Coordinates (Å) for Geometry Optimized Model of (3,5)F_2Y•

Atom	x	y	z
C	2.805212	1.237689	-0.015335
C	1.430973	1.236103	0.000950
C	0.630878	0.018905	0.010289
C	1.428465	-1.200143	0.001469
C	2.802520	-1.204658	-0.014803
C	3.514765	0.015868	-0.020695
C	5.020064	0.013824	0.000721
F	0.754192	-2.350176	0.005758
O	-0.617092	0.020063	0.022052
F	0.759396	2.387714	0.004759
H	3.333872	2.185881	-0.024350
H	3.329286	-2.153856	-0.023394
H	5.392645	0.000565	1.034703
H	5.429475	0.907432	-0.480707
H	5.427163	-0.869175	-0.502024

TABLE S7. Cartesian Coordinates (Å) for Geometry Optimized Model of (2,3,5)F_3Y•

Atom	x	y	z
C	2.790353	1.190079	0.063284
C	1.416173	1.220534	0.066203
C	0.622698	0.001163	0.001559
C	1.413218	-1.222654	-0.065211
C	2.788961	-1.231945	-0.067308
C	3.510436	-0.022412	-0.002829
C	5.012182	0.016017	-0.002644
F	0.733800	-2.366541	-0.126041
O	-0.623843	0.007989	0.003131
F	0.768634	2.379754	0.128884
F	3.480578	2.344443	0.124592
H	3.314712	-2.179651	-0.118664
H	5.392643	0.494278	0.908153
H	5.389904	0.605933	-0.846470
H	5.431364	-0.990951	-0.067247

TABLE S8. Cartesian Coordinates (Å) for Geometry Optimized Model of (2,3,6)F_3Y•

Atom	x	y	z
C	2.769442	1.216571	-0.061739
C	1.386802	1.224976	-0.060925
C	0.615697	-0.012143	0.003210
C	1.389595	-1.238734	0.065638
C	2.753414	-1.184354	0.061526
C	3.502028	0.022926	-0.001496
C	5.001381	-0.000054	-0.001497
H	0.858666	-2.181955	0.114743
O	-0.632998	0.010121	0.003066
F	0.731434	2.377805	-0.119250
F	3.424872	2.389011	-0.122159
F	3.473956	-2.322276	0.119519
H	5.380676	-0.476901	0.910289
H	5.408002	1.009869	-0.065613
H	5.378848	-0.588827	-0.845922

TABLE S9. Hyperfine values (MHz) for ring atoms of Y_{122}•. Values for fluorine atoms are shaded, whereas those for hydrogen are unshaded.

RNR β2 variant	**2**			**3**			**5**			**6**		
	A_x	A_y	A_z	A_x	A_y	A_z	A_x	A_y	A_z	A_x	A_y	A_z
wild type[a]	+5.0	+7.6	+2.1	-26.7	-8.4	-19.6	-26.7	-8.4	-19.6	+5.0	+7.6	+2.1
DFT Phen	+6	+10	+3	-27	-7	-21	-27	-8	-21	+6	+10	+3
(3,5)F_2Y	+5.3	+5.8	+8.5	-24	-10	+157	-24	-10	+157	+5.3	+6.3	+3
DFT (3,5)F_2-Phen	+5.5	+9	+3	-36	-24.5	+153	-36	-24.5	+153	+5.5	+9	+3
(2,3)F_2Y	+12	-4	-46	-18	-12.5	+178	-6	-27	-19	+6	+8	+2
DFT (2,3)F_2-Phen	+8.5	-3	-61	-37	-24	+165	-7	-27.5	-21	+5.5	+9.5	+3
(2,3,5)F_3Y	+8	-5	-37	-15	-12	+141	-24	-16	+187	+11	+8	+7
DFT (2,3,5)F_3-Phen	+6	-4	-45.5	-31.5	-21	+137.5	-42	-29	+183	+6.5	+10.5	+4
(2,3,6)F_3Y	+14	-11	-54	-22	-18	+210	-6	-21	-17	+12	-9	-36
DFT (2,3,6)F_3-Phen	+10.5	-2.5	-70	-46	-31	+209	-5.5	-21.5	-17	+4.5	-5	-42

[a] from Hoganson et al.[2]

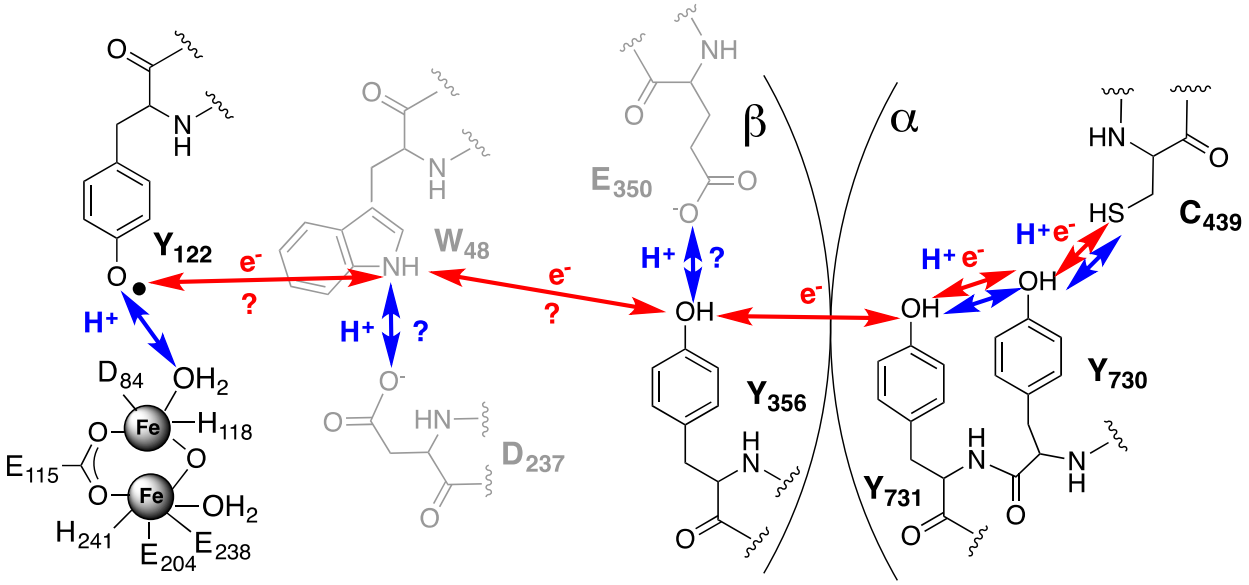

FIGURE S1. PCET pathway in *E. coli* class Ia RNR. The red and blue arrows represent the movement of electrons and protons through conserved aromatic amino acid residues (Y_{122}• → [W_{48}] → Y_{356} in β2 to Y_{731} → Y_{730} → C_{439} in α2). W_{48}, D_{237} and E_{350} are shown in gray, as there is currently no evidence for their involvement in PCET.

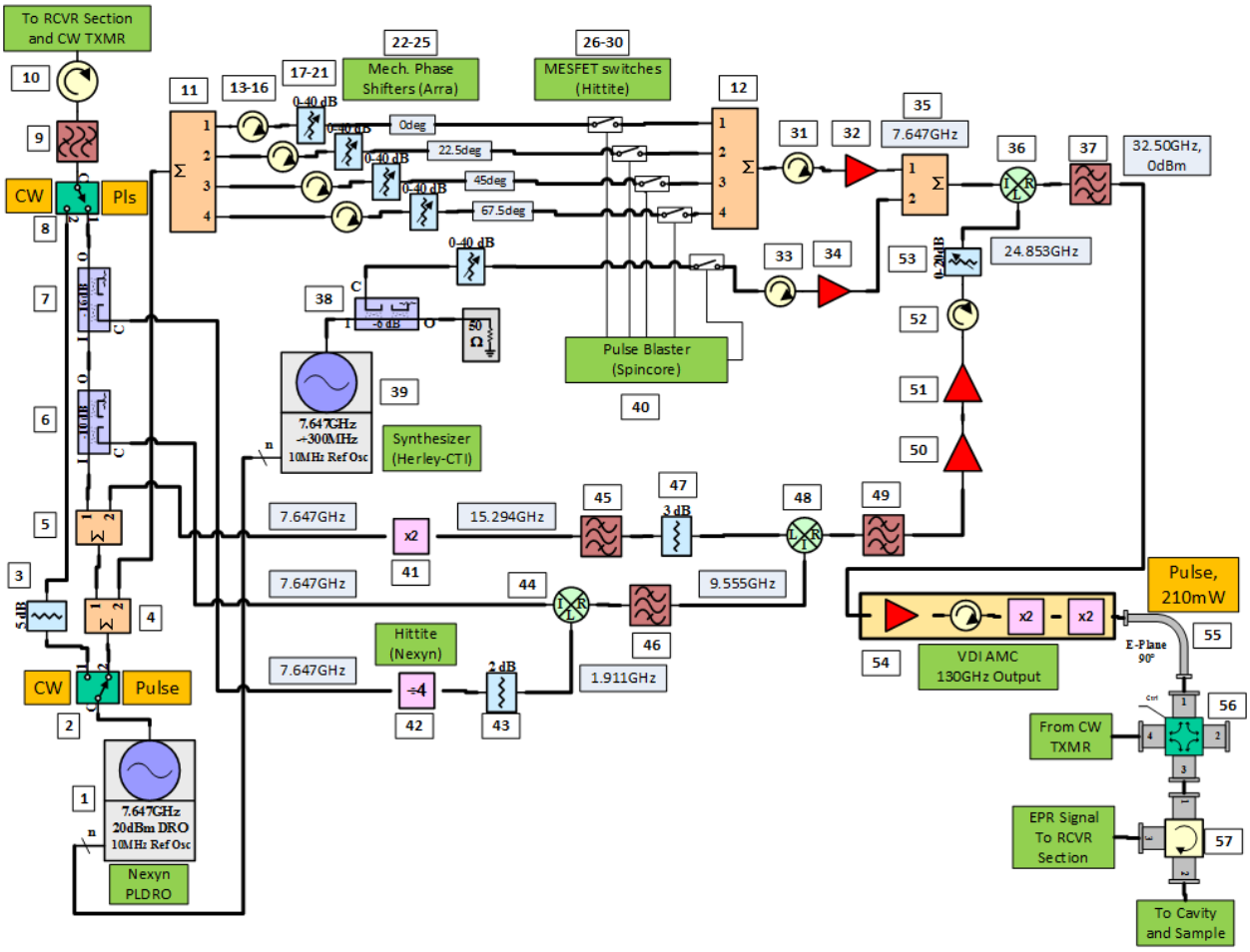

FIGURE S2. Block diagram of the modified and upgraded 130 GHz transmitter section of the original Krymov microwave bridge.

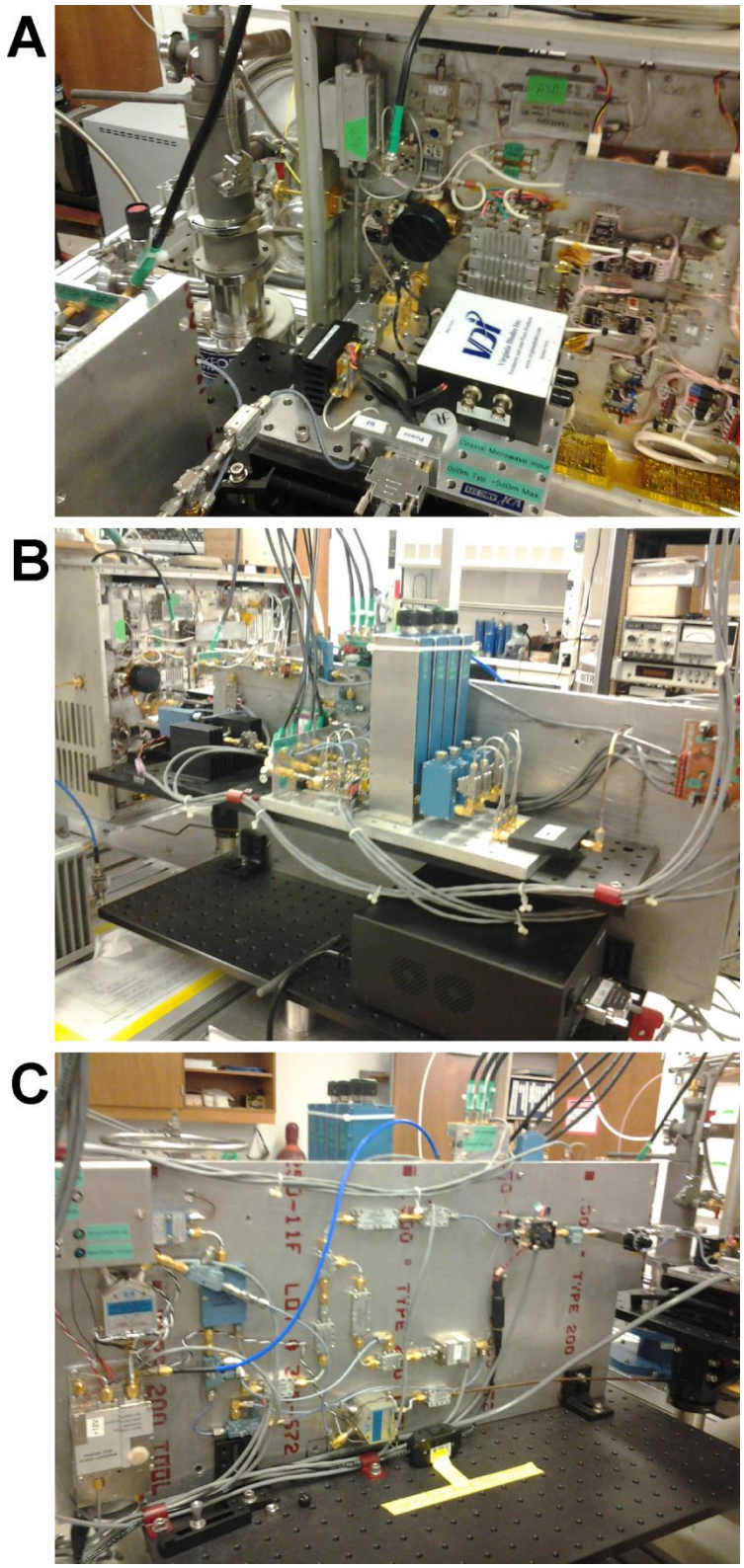

FIGURE S3. Photographs detailing the upgraded 130 GHz microwave bridge. A. The VDI AMC. B. The four pulse channels and fifth microwave synthesizer channel (hidden behind the blue phase shifters). C. The 7.647 GHz base frequency PLDRO and mix/multiply local oscillator side of the transmitter arm.

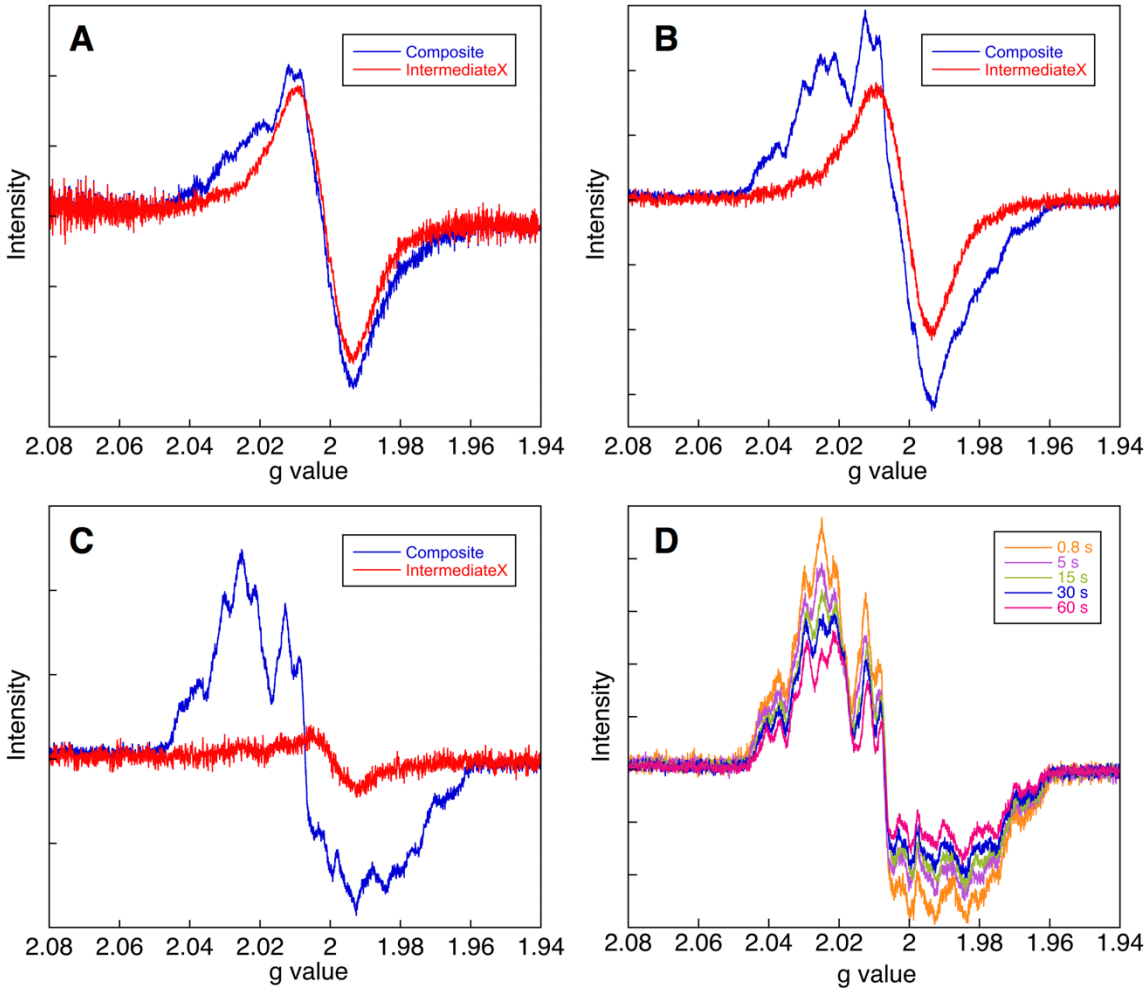

FIGURE S4. Reconstitution of the diferric-(2,3,6)F_3Y• monitored by RFQ-EPR spectroscopy. Subtraction of a scaled amount of the EPR spectrum of the 0.8 s sample (D, orange) from the composite spectrum at 23 ms (A), 83 ms (B) and 256 ms (C) revealed intermediate X (A, B and C, red). D. A total spin loss of ~ 40% is observed between the 0.8 s (orange) and 60 s samples (pink).

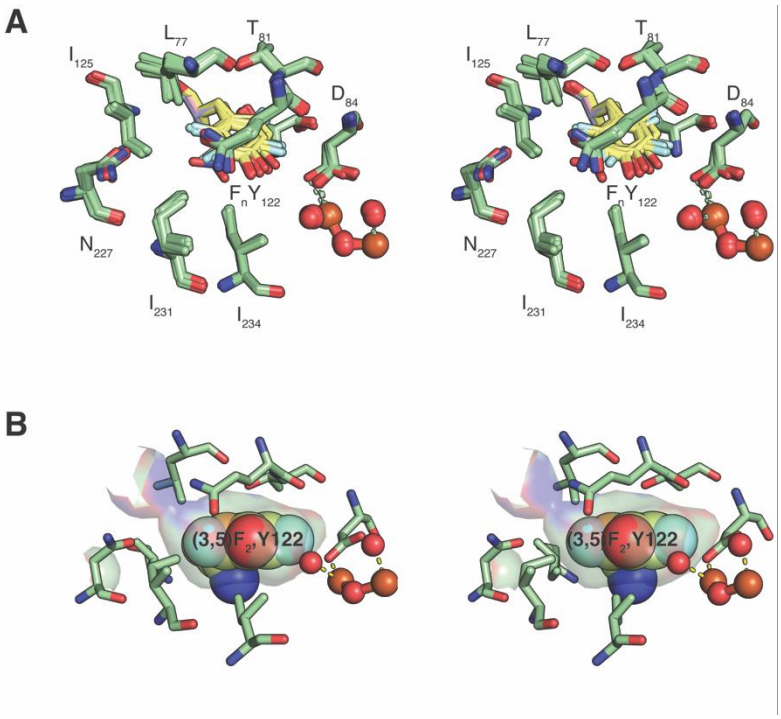

FIGURE S5. Uniformity of residues surrounding Y_{122} or F_nY_{122} variants. Colors are as in Figure 2 (main text). A. Overlay of all F_nY_{122} variant structures with three wt-β2 structures (PDB IDs 5CI4 [this work], 1RIB,[3] and 1MXR[4] and the structure of NO_2Y-β2 (pink, PDB ID 2XOF[5]). The residues in the hydrophobic pocket surrounding Y_{122} are shown. No changes are seen in the diferric cluster (shown in ball-and-stick representation) or in the conformation of any residue except Y_{122} and D_{84}. B. (3,5)F_2Y is shown in spheres with the van der Waals cavity surface shown for the surrounding residues. Rotation around χ_2 results in clashes in wt-β2 and all of the F_nY variants.

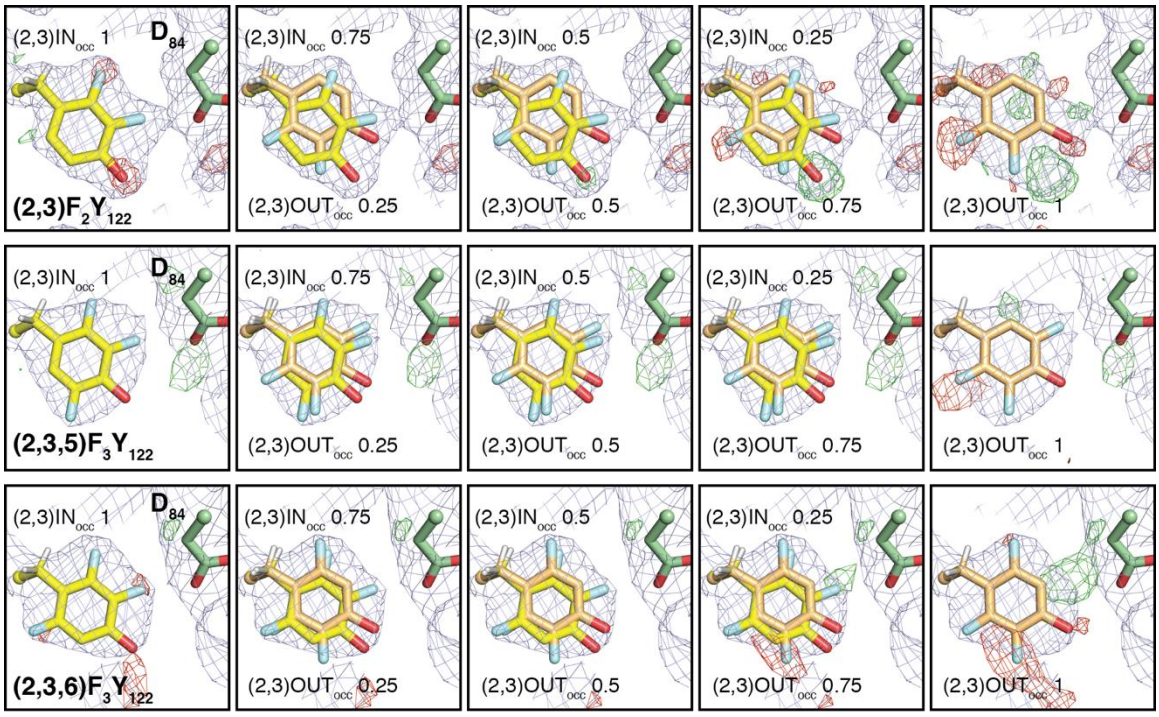

FIGURE S6. Evaluation of multiple conformations of F_nY_{122} variants. For each structure, mF_o-DF_c electron density was calculated after adjusting the occupancy of the two conformations to 1, 0.75, 0.5, 0.25 or 0, with the sum equal to 1. The conformations are designated (2,3)IN and (2,3)OUT corresponding to whether the (2,3)-fluorines are adjacent to D84 (IN) or facing away (OUT). Maps are shown contoured at 3 σ (green) or -3 σ (red). $2mF_o$-DF_c density is shown at 1 σ (blue). In each case, the (2,3)OUT conformation is clearly not preferred. For (2,3)F_2Y_{122} and (2,3,6)F_3Y_{122}, difference density is observed when the occupancy is full for either conformation. Modeling a mixture of the two conformations reduces the amount of difference density. The best maps were observed in the case of 0.75/0.25 IN/OUT for (2,3)F_2Y_{122} and 0.5/0.5 IN/OUT for (2,3,6)F_3Y_{122}. For (2,3,5)F_3Y_{122}, the IN conformation is favored over OUT, but the precise ratio is unclear.

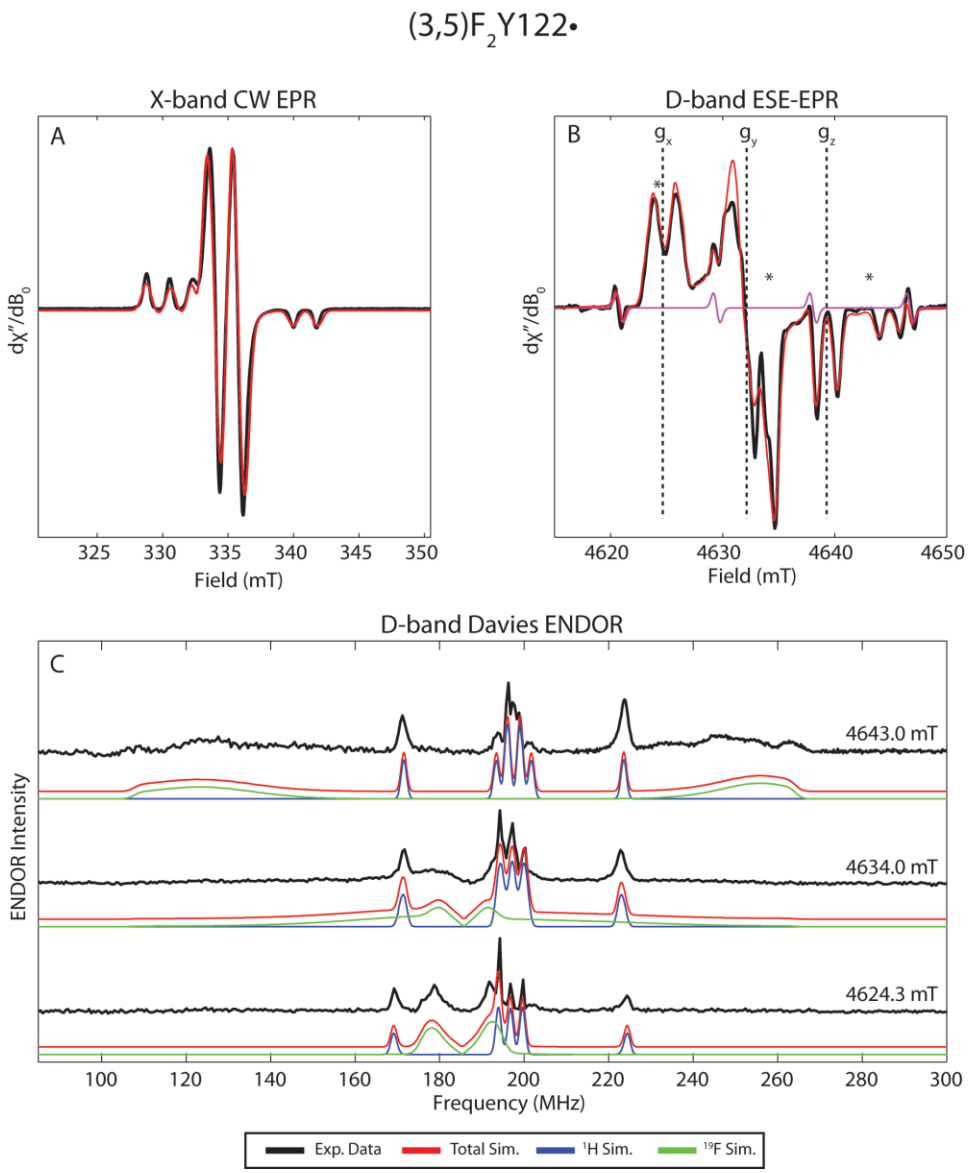

FIGURE S7. Combined X-band CW (Panel A), D-band Pulse EPR (Panel B) and ENDOR (Panel C) data sets of 3,5-F_2Y122•-β2. Black traces in all panels represent the experimental data, while red traces represent the spectral simulation using the parameters in Tables 6.4-6.8. The magenta trace in the pseudomodulated D-band spectrum represents the simulation of a signal from Mn(II) contamination with g = 2.00063 and ^{55}Mn A = 245 MHz. Asterisks indicate the three field positions at which Davies ENDOR was acquired. For the D-band Davies ENDOR, the simulations of ENDOR spectral contributions from ^{1}H and ^{19}F have been isolated in the blue and green traces, respectively.

Acquisition parameters: X-band CW EPR: Temperature = 80 K; MW Frequency = 9.395 GHz; MW Power = 317 μW; Modulation amplitude = 1.5 G; Modulation Frequency = 100 kHz; Conversion time = 50 ms. D-band ESE-EPR: Temperature = 30 K; MW Frequency = 129.996 GHz; $\pi/2_{MW}$ = 37.5 ns; τ = 200 ns; shot rep time (srt) = 10 ms. D-band Davies ENDOR: Temperature = 30 K; MW Frequency = 129.996 GHz; $\pi/2_{MW}$ = 37.5 ns; π_{RF} = 24 μs; τ = 300 ns; shot rep time (srt) = 10 ms.

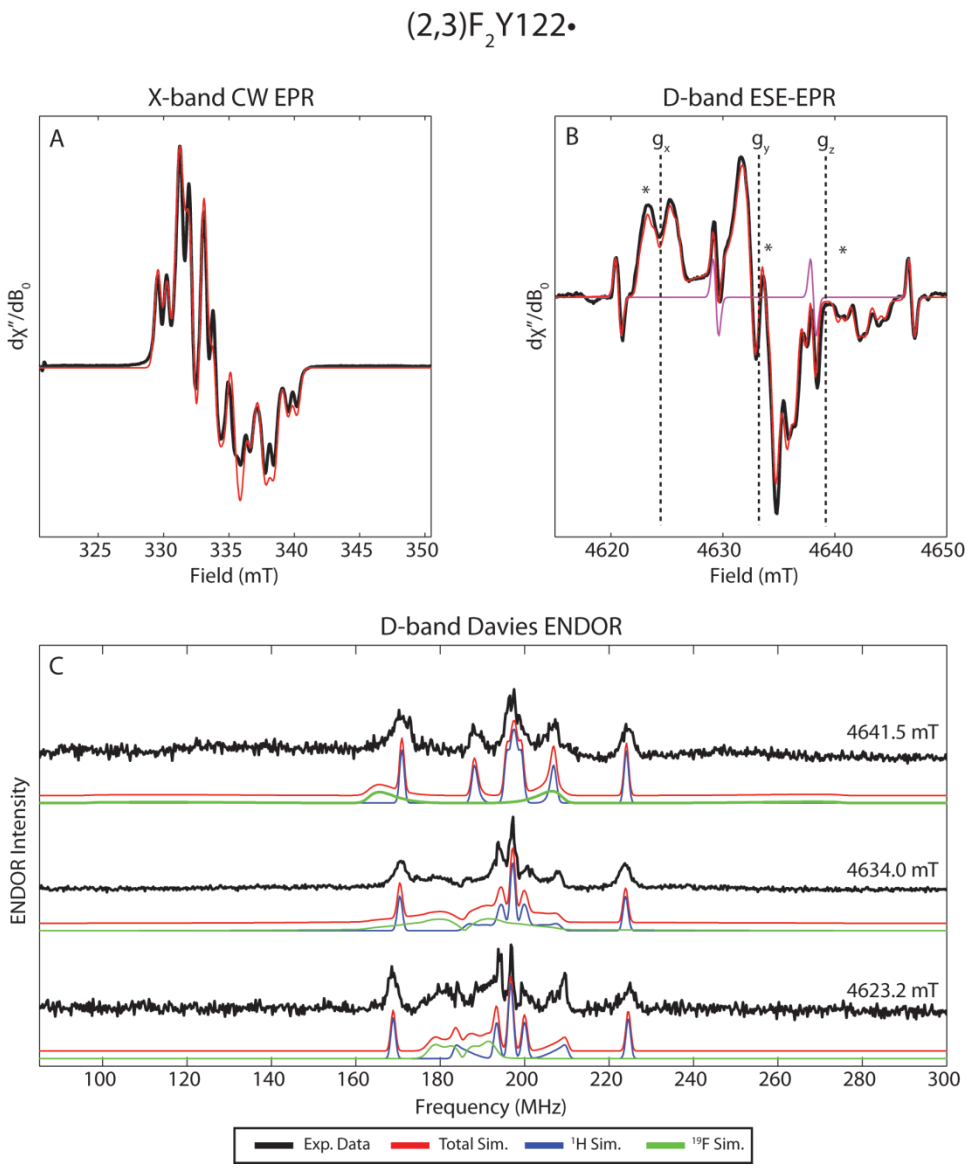

FIGURE S8. Combined X-band CW (Panel A), D-band Pulse EPR (Panel B) and ENDOR (Panel C) data sets of (2,3)F_2Y•-β2. Black traces in all panels represent the experimental data, while red traces represent the spectral simulation using the parameters in Tables 1, 2, and 3. The magenta trace in the pseudomodulated D-band spectrum represents the simulation of a signal from Mn(II) contamination with g = 2.00063 and ^{55}Mn A = 245 MHz. Asterisks indicate the three field positions at which Davies ENDOR was acquired. For the D-band Davies ENDOR, the simulations of ENDOR spectral contributions from ^{1}H and ^{19}F have been isolated in the blue and green traces, respectively.

Acquisition parameters: X-band CW EPR (Panel A): Temperature = 80 K; MW Frequency = 9.384 GHz; MW Power = 317 μW; Modulation amplitude = 1.5 G; Modulation Frequency = 100 kHz; Conversion time = 50 ms. D-band ESE-EPR (Panel B): Temperature = 30 K; MW Frequency = 129.996 GHz; $\pi/2_{MW}$ = 37.5 ns; τ = 200 ns; shot rep time (srt) = 10 ms. D-band Davies ENDOR (Panel C): Temperature = 30 K; MW Frequency = 129.996 GHz; $\pi/2_{MW}$ = 37.5 ns; π_{RF} = 24 μs; τ = 300 ns; shot rep time (srt) = 10 ms.

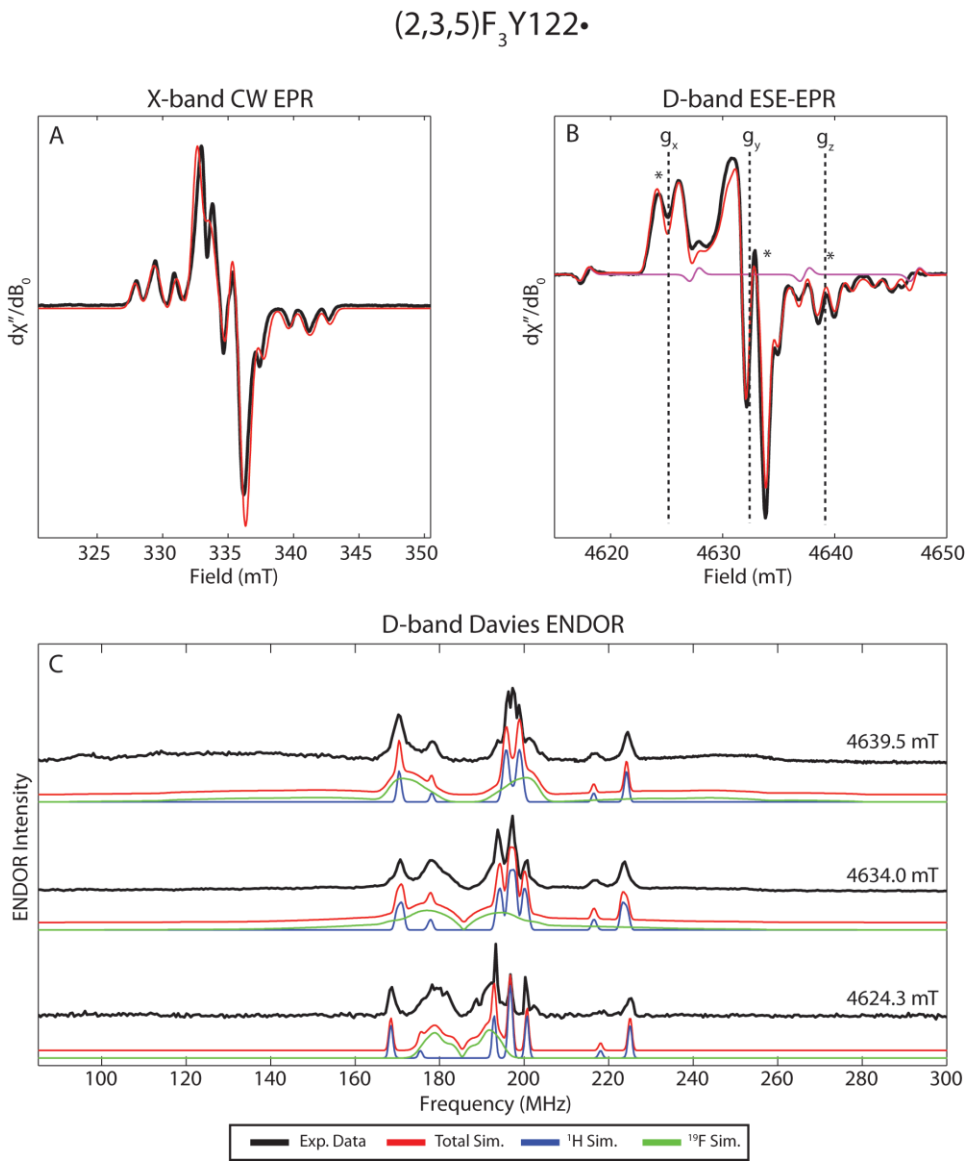

FIGURE S9. Combined X-band CW (Panel A), D-band Pulse EPR (Panel B) and ENDOR (Panel C) data sets of (2,3,5)F_3Y•-β2 .Black traces in all panels represent the experimental data, while red traces represent the spectral simulation using the parameters in Tables 1, 2, and 3. The magenta trace in the pseudomodulated D-band spectrum represents the simulation of a signal from Mn(II) contamination with g = 2.0007 and ^{55}Mn A = 276. Asterisks indicate the three field positions at which Davies ENDOR was acquired. For the D-band Davies ENDOR, the simulations of ENDOR spectral contributions from ^{1}H and ^{19}F have been isolated in the blue and green traces, respectively.

Acquisition parameters: X-band CW EPR (Panel A): Temperature = 80 K; MW Frequency = 9.397 GHz; MW Power = 317 μW; Modulation amplitude = 1.5 G; Modulation Frequency = 100 kHz; Conversion time = 50 ms. D-band ESE-EPR (Panel B): Temperature = 30 K; MW Frequency = 129.996 GHz; $\pi/2_{MW}$ = 37.5 ns; τ = 200 ns; shot rep time (srt) = 10 ms. D-band Davies ENDOR (Panel C): Temperature = 30 K; MW Frequency = 129.996 GHz; $\pi/2_{MW}$ = 37.5 ns; π_{RF} = 24 μs; τ = 300 ns; shot rep time (srt) = 10 ms.

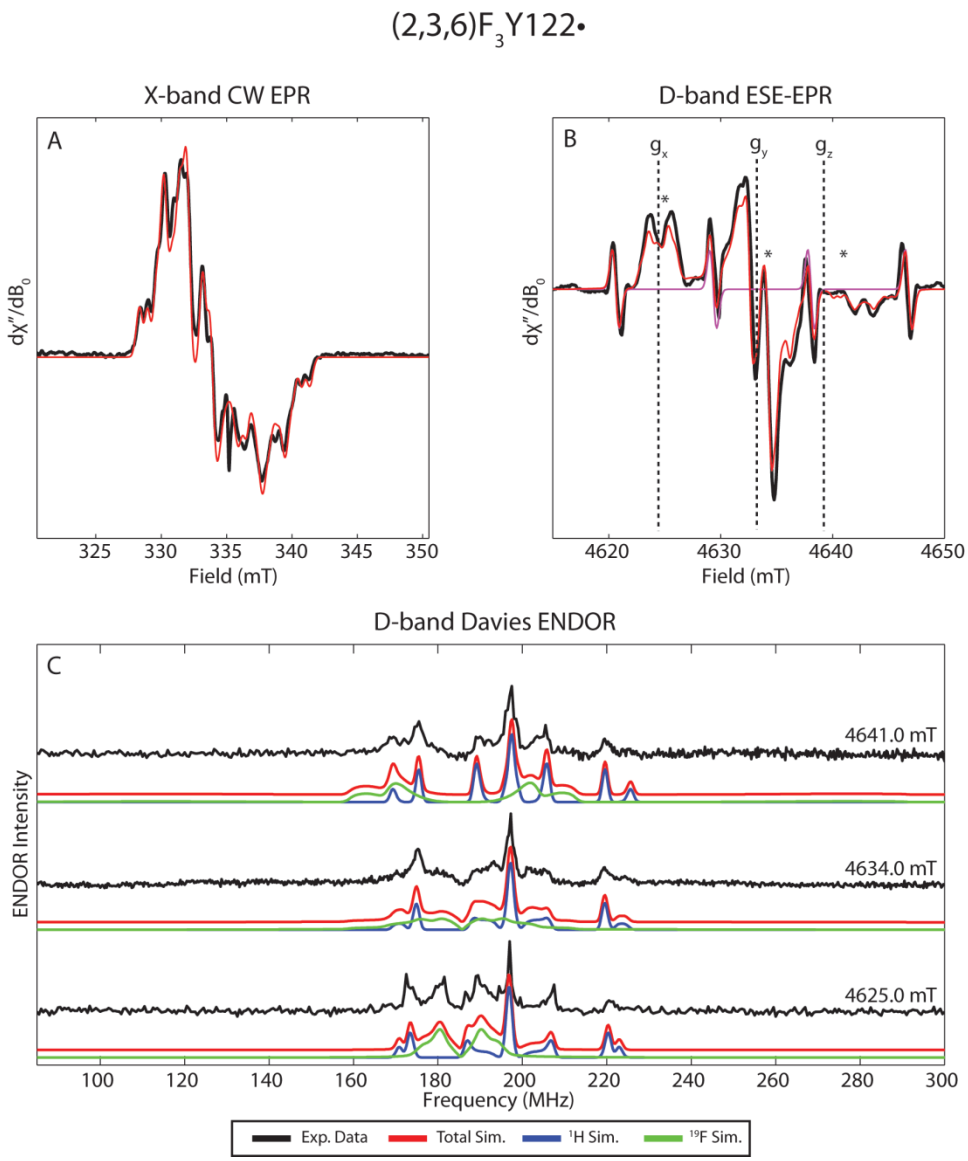

FIGURE S10. Combined X-band CW (Panel A), D-band Pulse EPR (Panel B) and ENDOR (Panel C) data sets of (2,3,6)F_3Y•-β2. Black traces in all panels represent the experimental data, while red traces represent the spectral simulation using the parameters in Tables 1, 2, and 3. The magenta trace in the pseudomodulated D-band spectrum represents the simulation of a signal from Mn(II) contamination with g = 2.00063 and ^{55}Mn A = 245 MHz. Asterisks indicate the three field positions at which Davies ENDOR was acquired. For the D-band Davies ENDOR, the simulations of ENDOR spectral contributions from ^{1}H and ^{19}F have been isolated in the blue and green traces, respectively.

Acquisition parameters: X-band CW EPR (Panel A): Temperature = 80 K; MW Frequency = 9.383 GHz; MW Power = 317 μW; Modulation amplitude = 1.5 G; Modulation Frequency = 100 kHz; Conversion time = 50 ms. D-band ESE-EPR (Panel B): Temperature = 30 K; MW Frequency = 129.996 GHz; $\pi/2_{MW}$ = 37.5 ns; τ = 200 ns; shot rep time (srt) = 10 ms. D-band Davies ENDOR (Panel C): Temperature = 30 K; MW Frequency = 129.996 GHz; $\pi/2_{MW}$ = 37.5 ns; π_{RF} = 24 μs; τ = 300 ns; shot rep time (srt) = 10 ms.

REFERENCES

(1) Bollinger, J. M., Jr.; Tong, W. H.; Ravi, N.; Huynh, B. H.; Edmondson, D. E.; Stubbe, J. A. *Methods Enzymol.* **1995**, *258*, 278.

(2) Hoganson, C. W.; Sahlin, M.; Sjöberg, B. M.; Babcock, G.T. *J. Am. Chem. Soc.* **1996**, *118*, 4672.

(3) Nordlund, P.; Eklund, H. *J. Mol. Biol.* **1993**, *232*, 123.

(4) Hogbom, M.; Galander, M.; Andersson, M.; Kolberg, M.; Hofbauer, W.; Lassmann, G.; Nordlund, P.; Lendzian, F. *Proc. Natl. Acad. Sci. USA* **2003**, *100*, 3209.

(5) Yokoyama, K.; Uhlin, U.; Stubbe, J. *J. Am. Chem. Soc.* **2010**, *132*, 15368.